Biomaterials 33 (2012) 6559–6569

Contents lists available at SciVerse ScienceDirect

Biomaterials

journal homepage: www.elsevier.com/locate/biomaterials

Simultaneous induction of autophagy and toll-like receptor signaling pathways by graphene oxide

Guan-Yu Chen [a], Hong-Jie Yang [a], Chia-Hsin Lu [a], Yu-Chan Chao [b], Shiaw-Min Hwang [c], Chiu-Ling Chen [a], Kai-Wei Lo [a], Li-Yu Sung [a], Wen-Yi Luo [a], Hsing-Yu Tuan [a,**], Yu-Chen Hu [a,d,*]

[a] Department of Chemical Engineering, National Tsing Hua University, 101, Sec. 2 Kuang Fu Rd., Hsinchu 300, Taiwan
[b] Institute of Molecular Biology, Academia Sinica, Taipei 115, Taiwan
[c] Bioresource Collection and Research Center, Food Industry Research and Development Institute, Hsinchu 300, Taiwan
[d] Institute of Biomedical Engineering, National Tsing Hua University, Hsinchu 300, Taiwan

ARTICLE INFO

Article history:
Received 26 April 2012
Accepted 27 May 2012
Available online 15 June 2012

Keywords:
Autophagy
Graphene oxide
Nanomaterials
Toll-like receptor
Signal transduction

ABSTRACT

Graphene oxide (GO) nanosheets have sparked growing interests in biological and medical applications. This study examined how macrophage, the primary immune cell type engaging microbes, responded to GO treatment. We uncovered that incubation of macrophage cell RAW264.7 with GO elicited autophagy in a concentration-dependent manner, as evidenced by the appearance of autophagic vacuoles and activation of autophagic marker proteins. Such GO-induced autophagy was observed in various cell lines and in macrophage treated with GO of different sizes. Strikingly, GO treatment of macrophage provoked the toll-like receptor (TLR) signaling cascades and triggered ensuing cytokine responses. Molecular analysis identified that TLR4 and TLR9 and their downstream signaling mediators MyD88, TRAF6 and NF-κB played pivotal roles in the GO-induced inflammatory responses. By silencing individual genes in the signaling pathway, we further unveiled that the GO-induced autophagy was modulated by TLR4, TLR9 and was dependent on downstream adaptor proteins MyD88, TRIF and TRAF6. Altogether, we demonstrated that GO treatment of cells simultaneously triggers autophagy and TLR4/TLR9-regulated inflammatory responses, and the autophagy was at least partly regulated by the TLRs pathway. This study thus suggests a mechanism by which cells respond to nanomaterials and underscores the importance of future safety evaluation of nanomaterials.

1. Introduction

Graphene and its oxidized form, graphene oxide (GO), have drawn intense attention in recent years for biological and medical applications [1]. The surface of GO contains hydrophilic oxygen-containing functional groups (i.e. hydroxyl, epoxyl and carboxyl tails) on the basal plane and edges, rendering GO amenable to stable dispersion in water and functionalization. These attributes have prompted the use of GO for bioimaging [2], cellular probing [3], cellular growth and differentiation [4], gene and drug delivery [5,6] and photothermal therapy [7]. These burgeoning applications in biomedicine entail the need to evaluate the *in vitro* and *in vivo* safety of GO.

Autophagy is a process that degrades intracellular components in response to stressful conditions (e.g. starvation and infection) and is linked to cellular processes as diverse as cell survival, cell death, pathogen clearance and antigen presentation [8–10]. Autophagy involves the formation of double-membraned vesicles termed autophagosomes, which sequester cytoplasm and organelles and then fuse with lysosomes to form autolysosomes, thus degrading the contents of the vacuole [10]. Autophagy is negatively controlled by mTOR (mammalian target of rapamycin) complex 1 (mTORC1) and inhibition of mTORC1 kinase activity initiates the formation of autophagosome that comprises a complex consisting of Beclin 1 and other factors. The autophagosome formation also involves the conversion of microtubule-associated protein light chain 3 (LC3-I) to the lipidated form LC3-II, consequently conversion from LC3-I to LC3-II is a common indicator of autophagy.

Toll-like receptors (TLRs) are important receptors for the detection of microbial antigens and subsequent induction of innate

* Corresponding author. Department of Chemical Engineering, National Tsing Hua University, 101, Sec. 2 Kuang Fu Rd., Hsinchu 300, Taiwan. Tel.: +886 3 571 8245; fax: +886 3 571 5408.
** Corresponding author. Tel.: +886 3 572 3661; fax: +886 3 571 5408.
E-mail addresses: hytuan@che.nthu.edu.tw (H.-Y. Tuan), ychu@mx.nthu.edu.tw (Y.-C. Hu).

0142-9612/$ – see front matter © 2012 Elsevier Ltd. All rights reserved.
doi:10.1016/j.biomaterials.2012.05.064

immune responses [11]. Among the TLRs, TLR2 recognizes bacterial lipoproteins while TLR3 detects virus-derived dsRNA. TLR4 recognizes lipopolysaccharides (LPS) and TLR5 recognizes bacterial flagellin. TLR7 mediates recognition of viral ssRNA while TLR9 senses unmethylated DNA with CpG motifs derived from bacterial and viruses [12]. Upon engagement with cognate ligands, the TLRs transduce signals by first recruiting adaptor proteins including myeloid differentiating factor 88 (MyD88) and TIR domain-containing adaptor inducing IFN-beta (TRIF), followed by activation of downstream signaling proteins such as TRAF6 and NF-κB, eventually resulting in various cellular responses including secretion of cytokines and interferons (IFNs).

The connection between autophagy and TLRs was discovered in 2007 as it was found that TLRs signaling in macrophages links the autophagy pathway to phagocytosis [13] and TLR4 stimulation enhances the autophagic elimination of phagocytosed mycobacteria in macrophages [14]. Ensuing studies further reported that TLR2, TLR3 and TLR7 play roles in autophagy induction [15,16]. The TLR-activated autophagy is regulated by the interaction of MyD88 or TRIF with Beclin 1 [17] and TLR engagement induces the interaction, thereby reducing the binding of Beclin 1 to inhibitory molecules. Beclin 1 also interacts with TRAF6 so as to facilitate its activation and subsequent formation of autophagosomes [18], thus TRAF6 seems to be crucial for TLR-activated autophagy [18]. The regulatory interaction of heat shock protein HSP90 with Beclin 1 is also required for autophagy induction downstream of TLR3 and TLR4 [19].

Since GO holds promise for diverse *in vivo* applications and macrophage is the primary immune cell type that engages foreign substances and modulates the immune responses *in vivo*, the overriding objective of this study was to explore how macrophage responded to GO treatment in order to evaluate the safety of GO.

2. Materials and methods

2.1. Preparation and characterization of GO

Large GO with a size of ≈2.4 μm was prepared from natural graphite (Bay Carbon, SP-1, average particle size ≈30 μm) by the modified Hummers method as described previously [20] and dispersed in water. The solution was centrifuged (7200 × g for 5 min) to remove unexfoliated GO and byproducts and centrifuged again (400 × g for 15 min) to remove broken fragments and debris. The pellet was dried under vacuum overnight to yield the large GO, weighed on a Sartorius SE2 ultra-micro balance with 0.1 μg resolution and dissolved in deionized water to a final concentration of 250 μg/ml. Small GO with a size of ≈350 μm was prepared via tip sonication (Misonix Sonicator 3000) of the large GO solution in an ice bath at a power of 30 W for 1 h, filtered through a 0.45 μm syringe filter (Sartorius Stedim Biotech) and dried under vacuum overnight. The small GO was weighed and dissolved in water to a desired concentration.

The surface morphology of GO was characterized with an atomic force microscope (AFM, XE-70, Park System) in tapping mode using the aluminum coating silicon probe (frequency 300 kHz, spring constants 40 N/m, scanning rate 1 Hz), under ambient conditions and scanning line of 512. High-resolution X-ray photoelectron spectroscopy (HRXPS) and attenuated total reflectance HRXPS were performed on a Kratos Axis Ultra DLD using a focused monochromatic Al X-ray source (1486.6 eV). The Fourier transform infrared (ATR-FTIR) spectra of GO were recorded using a Perkin–Elmer Spectrum RXI FTIR spectrometer with 2 cm^{-1} resolution and 32 scans, and the background was collected in the absence of samples. The size distribution of GO was characterized by using Dynamic Light Scattering (380 ZLS, Nicomp, USA) from Particle Sizing Systems at room temperature.

2.2. Cell culture and treatment with GO

The mouse macrophage cell line RAW264.7 was maintained in Dulbecco's modified Eagles medium (DMEM, Gibco) containing 10% fetal bovine serum (FBS, Gibco) and subcultured upon 70–80% confluency. For GO treatment, the cells were seeded to 6-well plates (3×10^5 cells/cm^2) overnight and cultured using the medium supplemented with GO at final concentrations of 5 or 100 μg/ml for 24 h. In parallel, the cells were treated with LPS (10 μg/ml, Sigma) for 24 h as the positive control. After the treatment, the cell morphology and vacuoles were observed under the phase contrast microscope.

2.3. Transmission electron microscopy (TEM)

The cells were harvested, centrifuged (215 × g, 10 min), washed with cold PBS and fixed with 2.5% glutaraldehyde (in 0.2 M sodium cacodylate, pH 7.4). The samples were then fixed in 1% OsO_4 for 1 h at 4 °C, dehydrated with increasing concentrations of ethanol, embedded in spur resin and sectioned. The ultrathin sections were stained with uranyl acetate and observed under the TEM.

2.4. Immunofluorescence microscopy

The cells were fixed and permeabilized as described previously [4], followed by extensive washing and primary antibody staining (1:100 dilution) for 1 h at 4 °C in the dark. The primary antibody was specific for LC3 (4108, Cell Signaling Technology), Beclin 1 (ab55878, Abcam), TLR4 (14-9924, eBioscience), TLR9 (ab17236, Abcam), MyD88 (ab2068, Abcam), TRAF6 (ab33915, bcam), phosphorylated NF-κB (3033, Cell Signaling Technology) or IRF3 (sc-15991, Santa Cruz Biotechnology). After washing, the cells were incubated with the goat anti-mouse antibody conjugated with Alexa 488 (for TLR9, Invitrogen), goat anti-rabbit antibody conjugated with Alexa 488 (for LC3, MyD88, TRAF6 and NF-κB, Invitrogen) or donkey anti-goat IgG conjugated with Dylight 488 (for IRF3, Jackson ImmunoResearch) for 1 h at 4 °C in the dark. After washing, the cells were counterstained with 4,6-diamidino-2-phenylindole (DAPI, Vector Labs) and visualized with a confocal microscope (Nikon TE2000 equipped with the confocal upgrade laser kit). Fifty to one hundred cells in the images for LC3 were counted for quantification of LC3+ cells.

2.5. ELISA and Western blot

At 24 h post-treatment, the supernatant was collected from the GO-treated cell culture and analyzed using ELISA kits specific for mouse IL-2, IL-10, TNF-α, IFN-β and IFN-γ. The cells were lysed for Western blot using primary antibodies (1:1000 dilution) specific for LC3, Beclin 1 or β-actin (A-2066, Sigma) and the secondary antibody was HRP-conjugated IgG (1:5000 dilution, Amersham Biosciences). The images were developed using the GeneGnome HR scanner (Syngene).

2.6. Reverse transcription-polymerase chain reaction (RT-PCR)

Total RNA was extracted from the cells using the NucleoSpin® RNA II purification kit (Clontech) and reverse transcribed to cDNA using the MMLV Reverse Transcriptase 1st-Strand cDNA Synthesis Kit (Epicentre Biotechnologies). The RT-PCR reactions were performed using Taq DNA polymerase (Promega) in the Px2 Thermal Cycler (Thermo Electron) under the condition of 30 s at 95 °C, 45 s at 60 °C and 30 s at 72 °C, and the amplicons were subjected to 2% agarose gel electrophoresis. For TLRs transcription analysis, the cDNA was amplified using the Murine TLR RT-Primers (Invivogen).

2.7. Flow cytometry

The cells were fixed and permeabilized with 4% formaldehyde and 0.5% Tween-20. After washing, the cells were incubated with the primary antibody (1:100 dilution) for 1 h at 4 °C in the dark. For TLR2 and TLR4 detection, the primary antibody was Alexa 488-conjugated MAb specific for mouse TLR2 (53-9024, eBioscience) or PE-conjugated MAb specific for mouse TLR4 (12-9924, eBioscience). For TLR7, TLR9, MyD88 and TRAF6 detection, the cells were incubated with the primary antibody specific for mouse TLR7 (ab45371, bcam), TLR9 (ab17236, bcam), MyD88 (ab2068, Abcam) or TRAF6 (ab33915, Abcam) and then incubated with Alexa 488-conjugated goat anti-rabbit (for TLR7, MyD88 and TRAF6) or goat anti-mouse (for TLR9) IgG for 1 h at 4 °C in the dark. After washing, the cells were collected for flow cytometry (FACSCalibur, BD Biosciences) analyses.

2.8. Gene knockdown by small interfering RNA (siRNA)

To knockdown specific genes, macrophages cells were transfected with 5 μg of scramble siRNA (SC-36869, Santa Cruz Biotechnology) or siRNA specific for TLR4, TLR9, MyD88, TRAF6 or TRIF (Santa Cruz Biotechnology). At 48 h post-transfection, cells were treated with GO or LPS as described above. The supernatant was collected 24 h later for ELISA and the cells were harvested for immunofluorescence microscopy and Western blot.

2.9. Statistical analysis

All data represented the mean ± standard deviation of at least 3 independent culture experiments. The data were statistically analyzed by one-way ANOVA. $p < 0.05$ was considered significant.

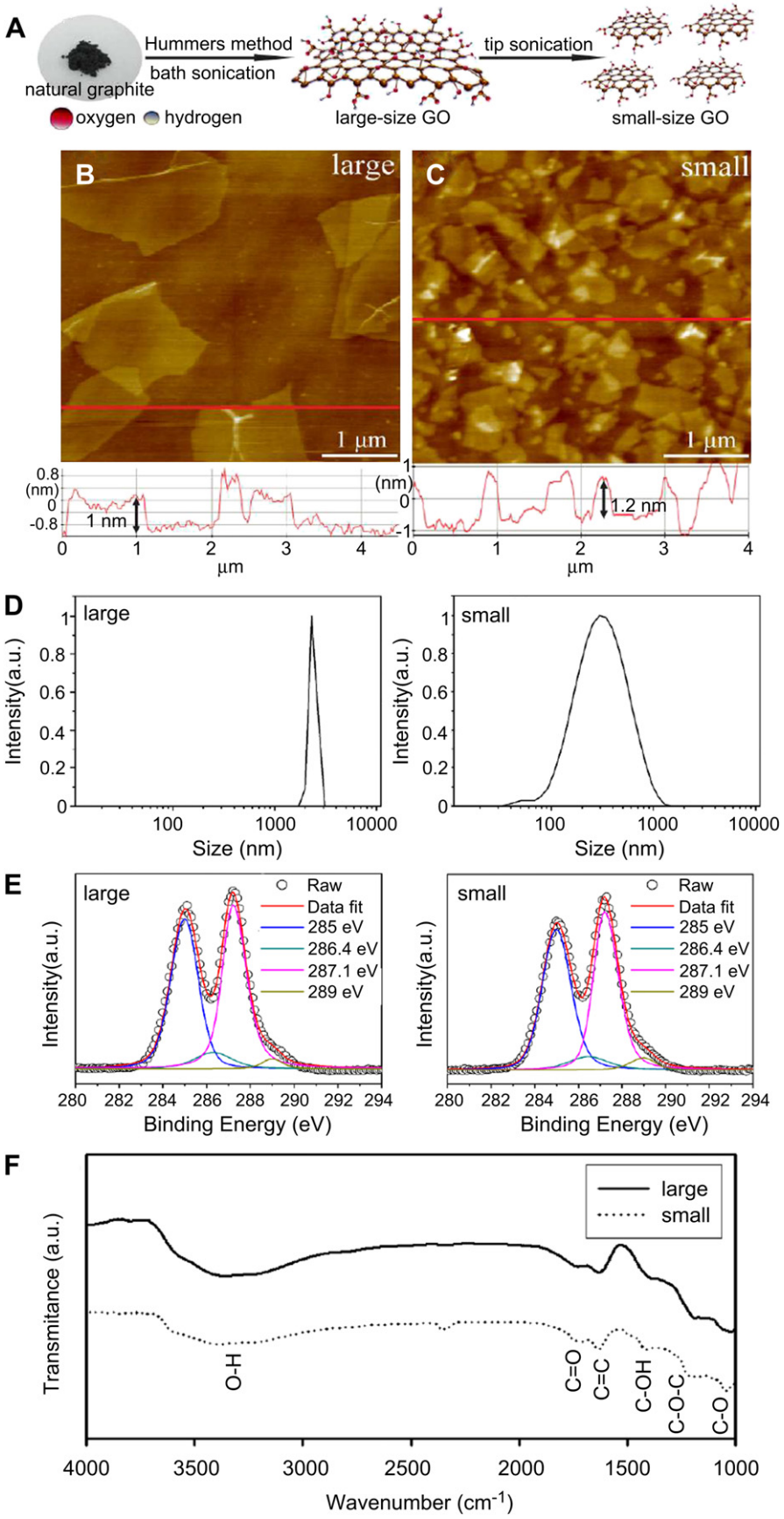

Fig. 1. Preparation and characterization of large and small GO nanosheets. (A) Schematic of preparation of GO of different sizes. (B–C) AFM images. (D) Dynamic light scattering analysis. (E) XPS spectra. (F) FTIR spectra.

3. Results

3.1. Preparation and characterization of large and small GO nanosheets

Fig. 1A schematically illustrates the preparation of GO nanosheets, for which large-size GO was prepared from natural graphite by the modified Hummers method as described [20] while small-size GO was obtained by sonicating large GO into smaller pieces via tip sonication. Atomic force microscopy (AFM) images showed significant difference of lateral dimensions between large and small GO (Fig. 1B–C). The thicknesses of both large and small GO measured ≈1.0–1.2 nm, which agreed with the GO thickness reported previously [21,22] and indicated the formation of single-layer GO. The GO was thicker than graphene (≈0.34 nm) due to the surface functional groups. The effective hydrodynamic diameters of large and small GO were ≈2.4 μm and ≈350 nm, respectively, as measured by Dynamic Light Scattering (Fig. 1D). The surface states of large and small GO were identical as demonstrated by high-resolution C 1s XPS spectra (Fig. 1E), in which the 4 peaks centering at 285, 286.4, 287.1 and 289.0 eV corresponded to C═C/C═C in the non-oxygenated aromatic rings, C–O (epoxy and alkoxy), C═O, and O═C–O groups, respectively [4]. The FTIR spectra (Fig. 1F) also delineated the same characteristic peaks of oxygen-containing groups for both large and small GO.

3.2. Autophagy induction by GO nanosheets

To examine how GO nanosheets influenced the macrophage, RAW264.7 cells were incubated with small GO at either 5 μg/ml (designated as GO5 group) or 100 μg/ml (designated as GO100 group) for 24 h. In comparison with the untreated control, GO5 induced the formation of small vacuoles inside the cells at 24 h post-incubation (Fig. 2A) but did not cause apparent cell death (Fig. S1A). Increasing the small GO concentration to 100 μg/ml (GO100 group) gave rise to more evident vacuole formation (Fig. 2A) and significant cell death (Fig. S1A), which were also observed in the LPS-treated cells (10 μg/ml). However, GO treatment did not elicit discernible apoptosis as illustrated by TUNEL assays (Fig. S1B). Similar vacuoles were also observed in the cells treated with large GO (Fig. S2A).

Since the GO-induced vacuoles were observed in cells treated with LPS, a ligand that induces both autophagy and TLR pathway [14,17], we surmised that GO-triggered autophagy. Indeed, the transmission electron microscopy demonstrated that GO5 evoked the appearance of some autophagic vacuoles (AV) while GO100 and LPS triggered more prominent AV (Fig. 2B). Notably, electron-dense materials within the AV were scarcely present in the LPS group but were abundant in the GO100 group (Fig. 2C), presumably due to the sequestered GO nanosheets.

Beclin 1 and LC3 are two key proteins associated with the autophagy pathway and are common indicators of autophagy

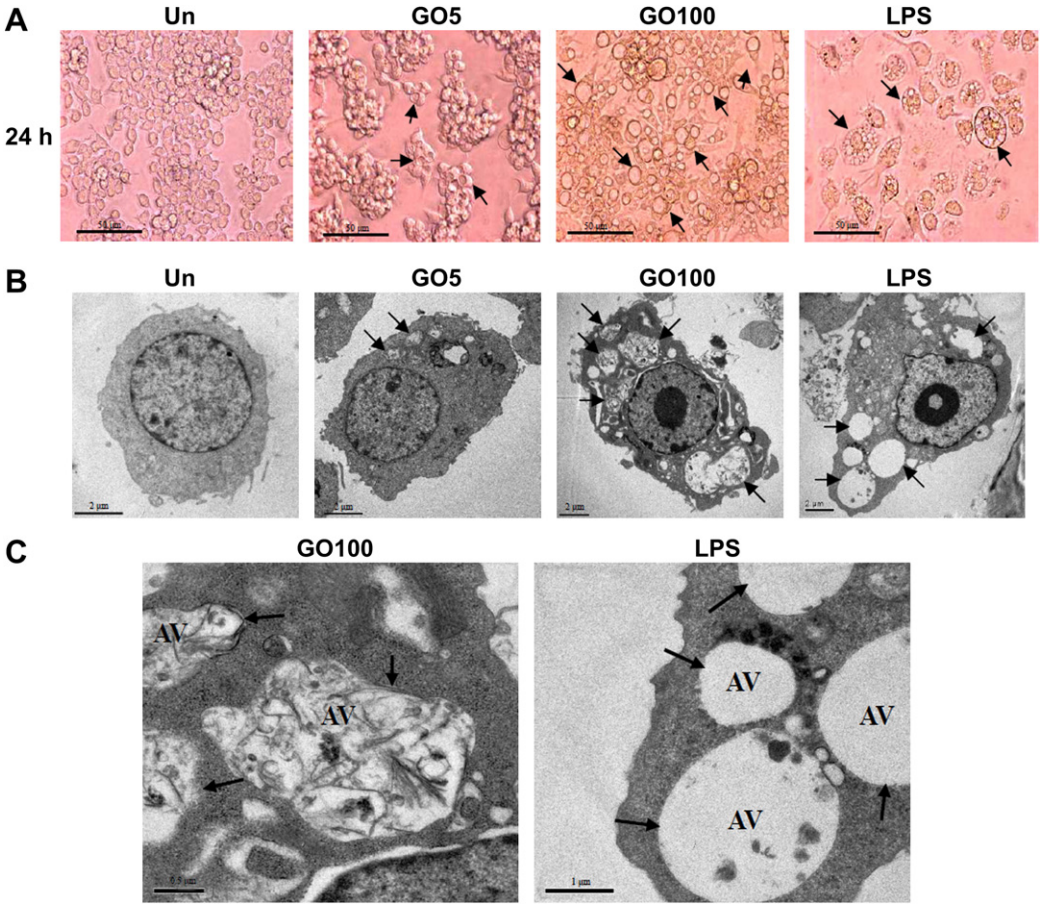

Fig. 2. GO induced the formation of autophagic vacuoles in macrophage. (A) Phase contrast micrographs (bar, 50 μm). (B) TEM images (bar, 2 μm). (C) Enlarged TEM images (bar, 1 μm). The macrophage cell (RAW264.7) was incubated with small GO at 5 μg/ml (GO5) or 100 μg/ml (GO100) for 24 h and examined by microscopy. In parallel, the cells were untreated or treated with LPS (10 μg/ml) for 24 h. Arrows indicate the autophagic vacuoles (AV).

induction [14,16,17,23,24]. LC3 is normally present diffusely in the cytosol but upon autophagy is converted from LC3-I (18 kD) to LC3-II (16 kD), accumulates on the autophagosome membrane and appears as dots [25]. Immunofluorescence microscopy for Beclin 1 and LC3 (Fig. 3A) showed that GO5 and GO100 provoked the appearance of many green dots, which were also observed in the LPS-treated cells but not in the untreated cells. The formation of such large aggregate dots similarly occurred in macrophages treated with large GO (100 μg/ml, Figs. S2B) or treated with dsDNA [24], and took place in stem cells treated with quantum dots [26]. Quantitative analysis of immunofluorescence micrographs (Fig. 3B) verified that GO100 triggered a significantly higher percentage of cells with LC3+ dots than the untreated, GO5 and LPS groups. Besides, pre-treatment of cells with the autophagy inhibitor 3-methyl adenine (3-MA) diminished the GO100-triggered formation of LC3+ aggregate dots (Fig. S3). Furthermore, Western blot (Fig. 3C) not only attested that small GO provoked the expression of both Beclin 1 and LC3, but also revealed the emergence of LC3-II, thus confirming the LC3 ligation to autophagosome. These data altogether proved the induction of autophagy in macrophages by large and small GO in a concentration-dependent manner.

3.3. Elicitation of cytokine expression and TLR4/TLR9 signaling

Since the interplay between autophagy and TLRs signaling was recently revealed, we were inspired to explore whether GO elicited TLRs-associated inflammatory responses. ELISA analysis (Fig. 4) depicted that treatment of macrophage cells with small GO at 100 μg/ml significantly induced the production of IL-2, IL-10, IFN-γ and TNF-α when compared with the untreated cells. Such cytokine response was GO concentration-dependent and concurred with the cytokine secretion triggered by LPS. However, treatments of macrophage with small GO at 5 and 100 μg/ml did not elicit the secretion of IFN-β.

Conversely, GO5 and GO100 evidently upregulated the transcription of TLR9 but barely triggered other TLRs genes, as depicted by RT-PCR analyses (Fig. 5A). Since TLR2, TLR4 and TLR7 also induce autophagy [14–16], we further assayed the upregulation of these TLRs in addition to TLR9, by immunofluorescence labeling coupled with flow cytometry. Fig. 5B reveals that GO100 only marginally induced the expression of TLR2 and TLR7, but pronouncedly upregulated the TLR4 and TLR9 expression. The upregulation of TLR4 and TLR9 by GO100 was further confirmed by immunofluorescence microscopy (Fig. 5C–D). Treatment of macrophage cells with large

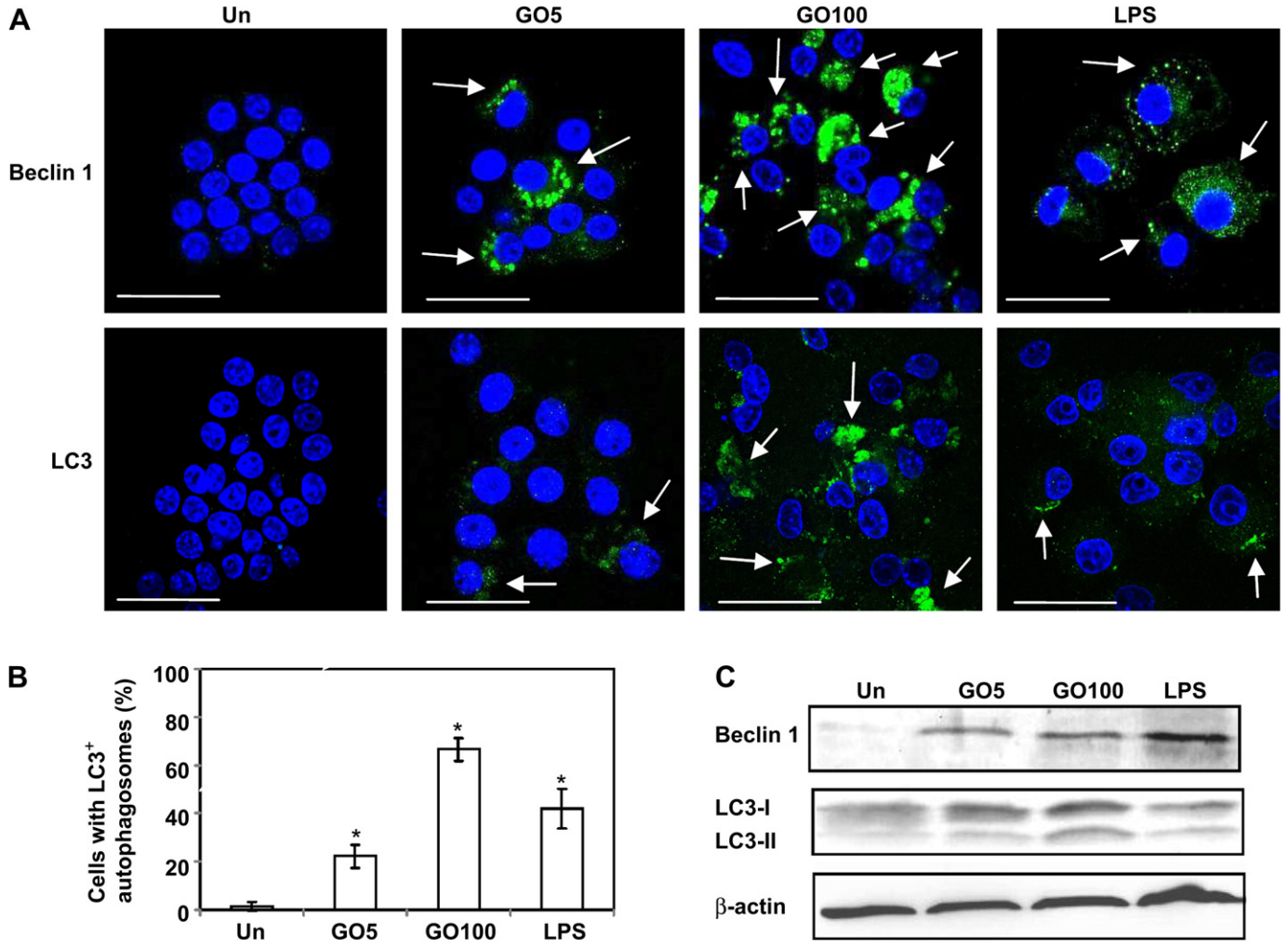

Fig. 3. GO-induced autophagy in macrophage. (A) Immunofluorescence microscopy for Beclin 1 and LC3. (B) Percentage of cells with LC3+ autophagosomes as determined from quantitative analysis of immunofluorescence microscopic images. (C) Western blot analysis of Beclin 1 and LC3. Bar, 100 μm. The number of LC3+ dots was scored on 50–100 cells. $^{*}p < 0.05$.

GO at 100 μg/ml likewise provoked remarkable upregulation of TLR4 and TLR9 (Fig. S4).

Since only the expression of TLR4 and TLR9 was markedly elicited by GO, we next examined the roles of TLR4 and TLR9 pathways on the inflammatory response. The TLR4 pathway signals through either TRIF or MyD88. The TRIF-dependent pathway results in activation and nuclear translocation of IRF3, thereby triggering the secretion of IFN-α/β [11]. However, GO5 and GO100 neither evoked nuclear translocation of IRF3 (Fig. S5) nor elicited IFN-β expression (Fig. 4), thus indicating the dispensable role of IRF3.

Conversely, TLR4 signaling through MyD88 leads to the formation of MyD88/IRAK4/TRAF6 signalsome, nuclear translocation of phosphorylated NF-κB and subsequent cytokine expression [27]. TLR9 stimulation recruits MyD88 and results in the formation of MyD88/IRAK4/TRAF6/TRAF3 complex, which relays signals either through IRF7 for IFN-α/β secretion, or through NF-κB for cytokine expression [28]. As demonstrated by the flow cytometry (Fig. 6A–B) and immunofluorescence microscopy (Fig. 6C–D), GO100 upregulated the expression of MyD88 and TRAF6 and formation of aggregates indicative of signalsome complex. Concomitantly, GO100 led to the activation and nuclear translocation of phosphorylated NF-κB (Fig. 6E). In conjunction with the cytokine expression downstream of NF-κB signaling (Fig. 4), Figs. 5 and 6 collectively suggested that GO100 activated the TLR4 and TLR9 signaling cascades.

3.4. Roles of TLR4/TLR9 pathways on the GO-induced cytokine response and autophagy

To confirm the roles of individual signaling mediators on the cytokine response, the macrophage cells were treated with siRNA specific for TLR4, TLR9, MyD88, TRIF or TRAF6. Following the silencing as confirmed by RT-PCR (Fig. 7A–B), the macrophages cells were incubated with GO100 as in Fig. 4. ELISA analysis (Fig. 7C) depicted that silencing TLR4, TLR9, MyD88 and TRAF6 attenuated the IFN-γ and TNF-α expression with statistical significance ($p < 0.05$) when compared with the

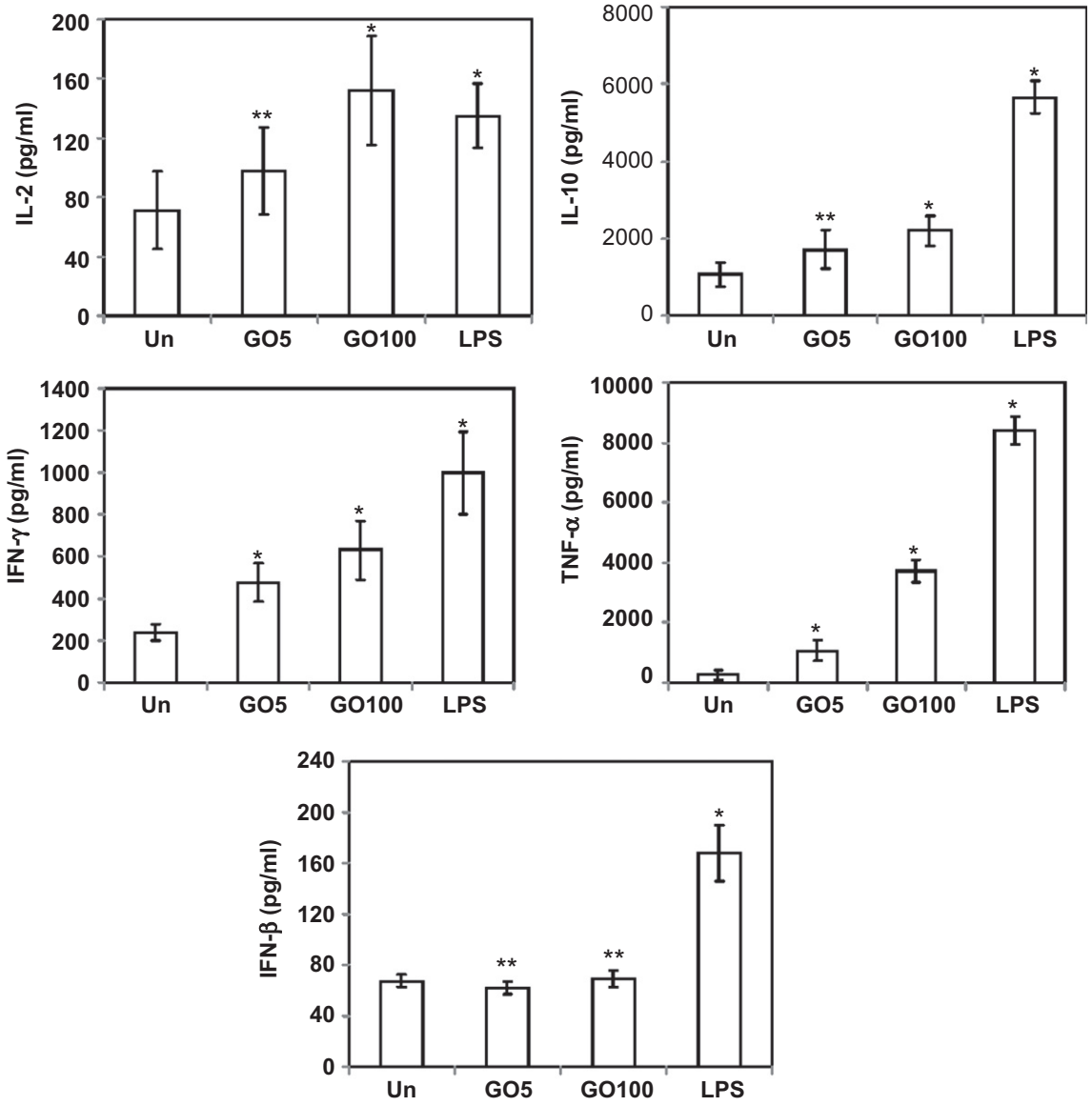

Fig. 4. Cytokine expression by GO-treated macrophage. RAW264.7 cells were untreated or treated with GO5 or GO100 for 24 h as in Fig. 2 and the cytokine secretion was measured using ELISA kits. The LPS-treated cells served as the positive control. $^{*}p < 0.05$; $^{**}p > 0.05$.

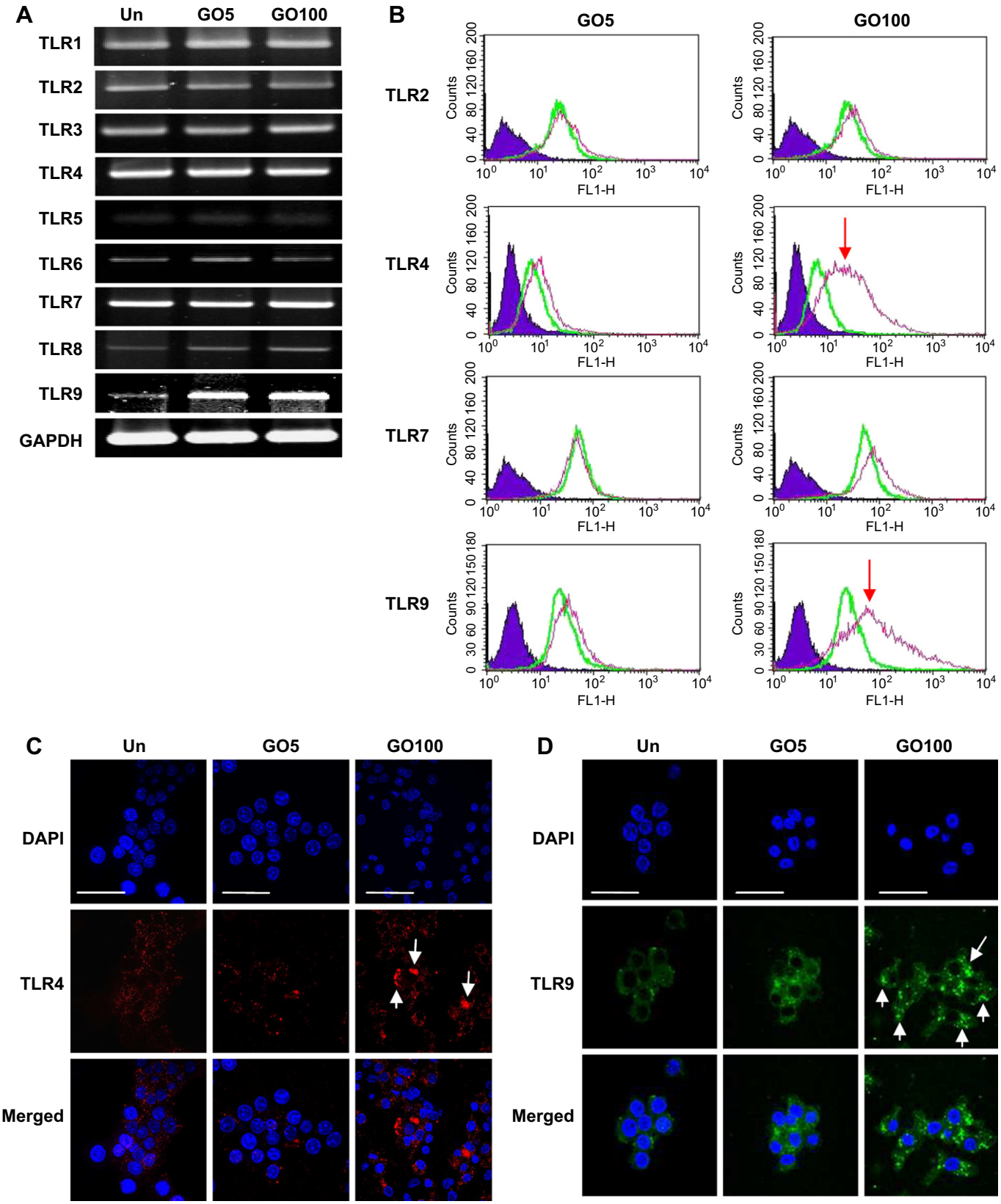

Fig. 5. GO treatment of macrophage triggered the TLR4 and TLR9 activation. (A) RT-PCR analysis of TLRs mRNA levels. (B) Flow cytometry analysis of TLRs expression. The green and purple lines indicate the untreated and treated cells, respectively. (C–D) Immunofluorescence microscopic analysis of TLR4 and TLR9. RAW264.7 cells were treated with GO5 or GO100 for 24 h, immunostained with anti-TLR antibodies and subjected to analysis. Magnification, 1000×. Bar, 100 μm. (For interpretation of the references to color in this figure legend, the reader is referred to the web version of this article.)

control treated with scramble siRNA, thereby attesting the roles of TLR4, TLR9 and their downstream MyD88-dependent pathway in the GO-triggered inflammatory response. In contrast, silencing TRIF did not significantly diminish the IFN-γ and TNF-α expression, nor was IFN-β expression attenuated by silencing these genes (Fig. 7C), thereby suggesting the dispensable role of TRIF-dependent pathway in the GO-triggered innate responses.

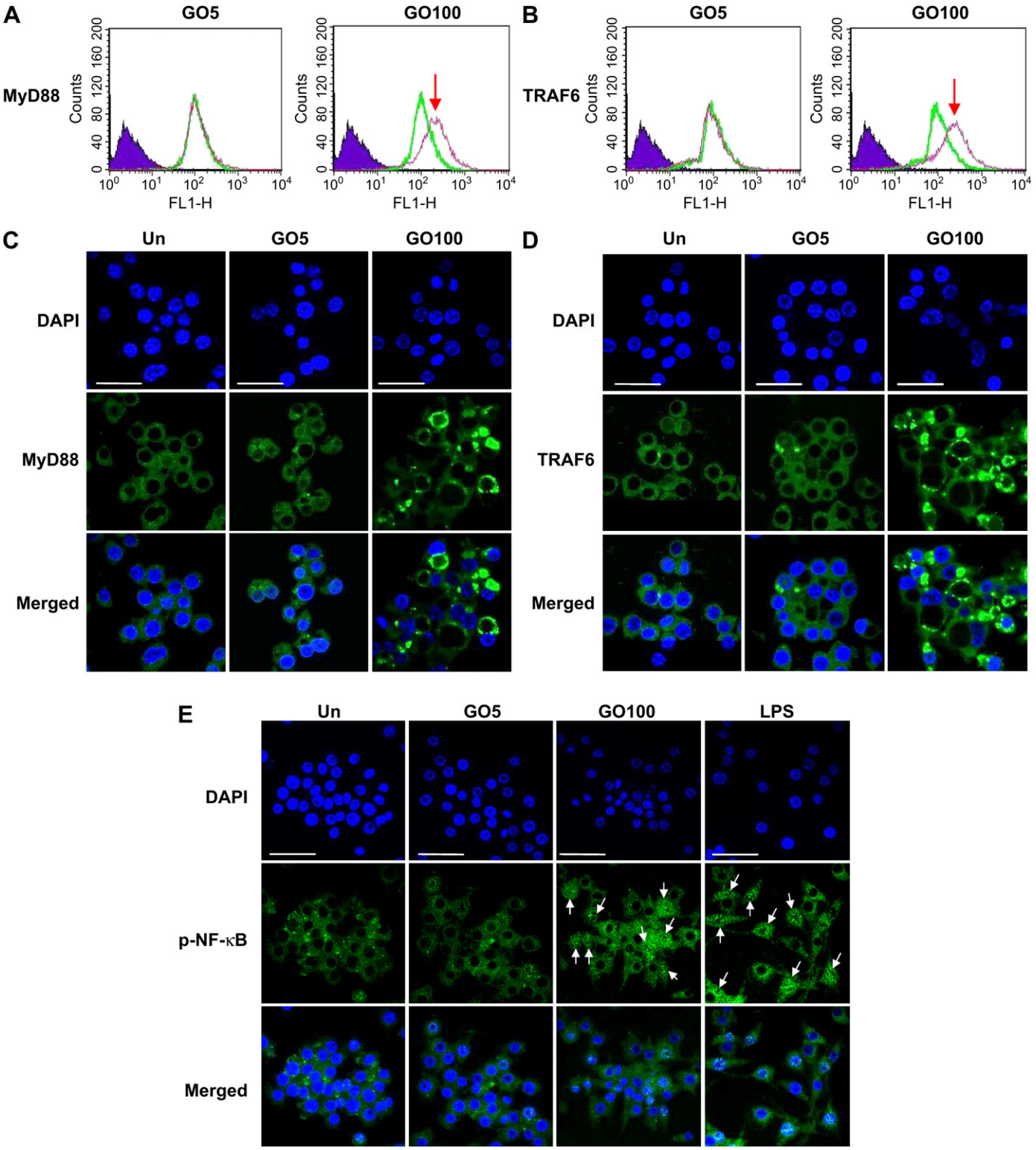

Fig. 6. GO treatment activated the TLR4/TLR9 signaling cascade. (A–B) Flow cytometry analysis of MyD88 and TRAF6 expression. (C–D) Immunofluorescence microscopic analysis of MyD88 and TRAF6. (E) Immunofluorescence microscopic analysis for nuclear translocation of NF-κB. Arrows indicate the NF-κB within the nucleus. RAW264.7 cells were untreated or treated with small GO for 24 h as in Fig. 2 and immunostained with antibodies specific for MyD88, TRAF6 or phosphorylated NF-κB for analysis.

Immunofluorescence microscopy (Fig. 7D) further illustrated that silencing TLR4, TLR9, TRIF, MyD88 and TRAF6 abolished the GO-induced formation of Beclin 1 aggregates. Similar inhibition of GO-induced LC3+ aggregates also occurred after silencing TLR4, TLR9, TRIF, MyD88 and TRAF6, as confirmed by immunofluorescence microscopy (Fig. 7E) and quantitative analysis (Fig. 7F). The Western blot (Fig. 7G) further confirmed that silencing these genes suppressed Beclin 1 expression and LC3-I conversion to LC3-II.

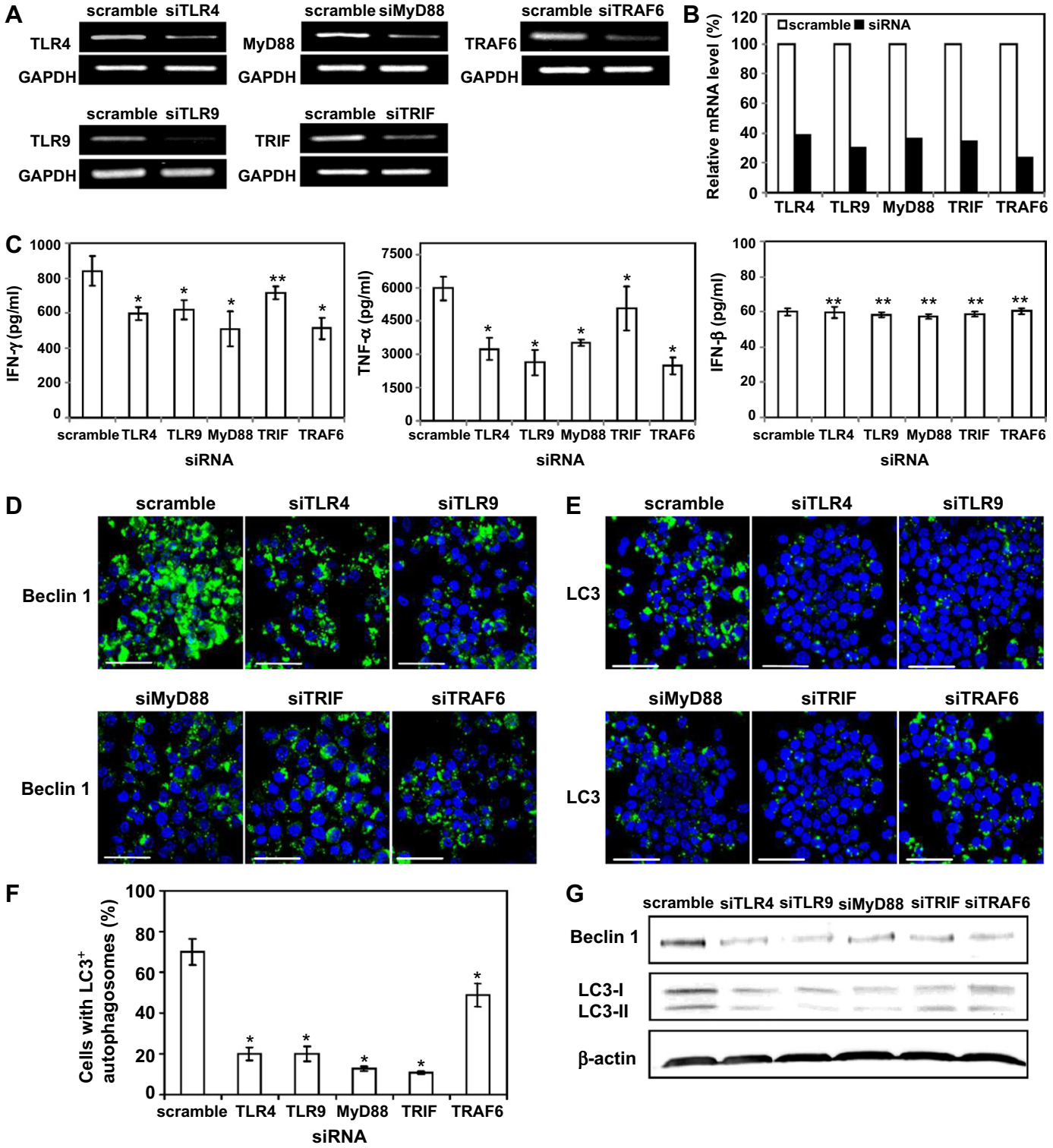

Fig. 7. Silencing the signaling mediators in the TLR4/TLR9 pathway diminished the GO-induced cytokine secretion and autophagy. (A–B) Confirmation of gene knockdown by RT-PCR and semi-quantitative analysis. (C) Cytokine expression. (D–E) Immunofluorescence microscopic analysis of Beclin 1 and LC3. (F) Quantitative analysis of LC3+ cells. (G) Western blot analysis of Beclin 1, LC3-I and LC3-II. RAW264.7 cells were transfected with a scramble siRNA or siRNA specific for TLR4, TLR9, MyD88, TRIF or TRAF6 for 48 h, followed by GO100 treatment for 24 h. after GO100 treatment, the media were harvested for ELISA analysis of IFN-γ, TNF-α or IFN-β. The cells were harvested for RT-PCR, immunofluorescence microscopy or Western blot analysis. Bar, 100 μm $^{*}p < 0.05$; $^{**}p > 0.05$.

These data altogether indicated that blockade of TLR4, TLR9 and their downstream MyD88- and TRIF-dependent signaling could abrogate the GO-induced autophagy.

4. Discussion

Recent publications have shown that nanomaterials such as quantum dots [26], polymer dendrimers [29], fullerene [30], gold nanoparticles [31], carbon nanotube [32] and αAl_2O_3 nanoparticles [25] can induce autophagy. However, the underlying mechanisms contributing to the nanomaterials-induced autophagy remain elusive. Very recently, GO nanosheets with different lateral dimensions ($\approx$2 μm and 350 nm) were found to be internalized by macrophages via phagocytosis, resulting in cell death and inflammatory responses [33], but whether GO induces autophagy has yet to be reported. Here we prepared both large (size $\approx$ 2.4 μm) and small (size $\approx$ 350 nm) GO nanosheets (Fig. 1) and uncovered that GO-triggered cell death (Fig. S1) and autophagy (Figs. 2 and 3) in a concentration-dependent manner. Such GO-induced autophagy was observed in macrophages treated with large and small GO nanosheets, probably because large and small GO could be internalized by macrophages with equal efficiencies [33]. Furthermore, autophagy was induced by GO100 in various cell types (Fig. S6) including liver cancer cells (SNU-449 and mahlavu), lung cancer cell (A549) and human embryonic kidney cell (HEK293), proving that GO-induced autophagy is not restricted to macrophage.

TLRs are generally considered as sensors of biological molecules such as nucleic acids, proteins and polysaccharides [12,34]. Strikingly, we discovered for the first time that treatment of cells with a non-biological material such as GO also triggered the secretion of cytokines (IL-2, IFN-γ, IL-10 and TNF-α) mediated by TLR4 and TLR9 (Figs. 3–6 and 7A–C). The cytokine expression profile was consistent with that of macrophage cells treated with GO of different lateral sizes [33]. Notably, the GO-induced TLRs signaling neither elicited IFN-β expression nor activated IRF3, and TRIF silencing failed to abolish the response, suggesting that TRIF and its downstream IRF3 were dispensable in the GO-elicited inflammatory response (Fig. 8). In contrast, GO treatment triggered upregulations of TLR4, TLR9, MyD88, TRAF6, NF-κB, and silencing of TLR4, TLR9, MyD88 and TRAF6 suppressed the cytokine expression (Figs. 3–6 and 7A–C). As such, GO treatment led to the activation of TLR4 and TLR9, which relayed signals through MyD88/TRAF6/NF-κB and ultimately gave rise to cytokine expression (Fig. 8). Since macrophage is one primary immune cell type resident in tissues, our data suggested that *in vivo* administration of GO at high concentration may elicit TLR4- and TLR9-mediated cytokine responses (e.g. induction of TNF-α, IFN-γ and IL-2) that can modulate ensuing adaptive immune responses, thus these findings underscore the importance of further scrutinizing safe application of GO *in vivo*.

Another striking finding was that the GO-induced autophagy was modulated by TLR4 and TLR9 signaling pathways (Fig. 7D–F). To date the precise mechanisms regulating the TLRs-elicited autophagy remain to be established [10] although agonists stimulating TLR2, TLR3, TLR4 and TLR7 were shown to trigger autophagy [15,16,18,24]. Based on one plausible mechanism that links TLR4 signaling and autophagy [23], Beclin 1 is inactivated by the inhibitory molecules (e.g. Bcl-2) in the usual state [19]. After TLR4 engagement, MyD88 and TRIF are activated and Beclin 1 is dissociated from the inhibitory molecules. Downstream of MyD88 or TRIF, TRAF6 activates Beclin 1 to initiate the autophagic processes [35]. However, Beclin 1 is not a signaling molecule in TLR-mediated NF-κB activation and IFN-β induction [19]. Now that silencing TLR4,

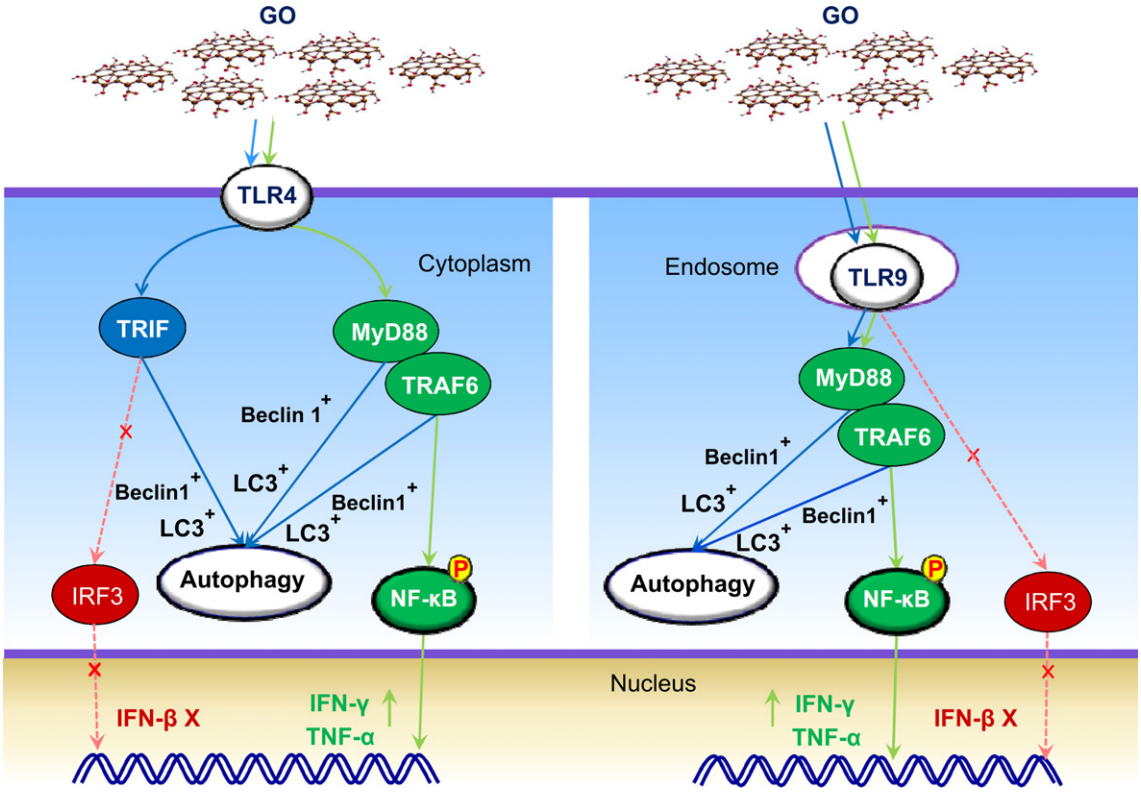

Fig. 8. Overview of the GO-induced cytokine response and autophagy mediated by the TLR4/TLR9 signaling pathway. GO treatment led to the activation of TLR4 and TLR9, which relayed signals through MyD88-TRAF6-NF-κB and ultimately gave rise to cytokine expression. However, GO-induced TLRs signaling neither elicited IFN-β expression nor activated IRF3, suggesting that TRIF and IRF3 were dispensable in the inflammatory response. Conversely, GO-induced TLR4-MyD88-TRAF6 and TLR4-TRIF signaling cascades signaled through Beclin 1 to initiate autophagy. GO engagement of TLR9 also activated MyD88 and TRAF6, leading to Beclin 1 and LC3 activation and subsequent autophagy.

MyD88, TRIF and TRAF6 attenuated the GO-induced autophagy (Fig. 7D–G), our data suggested that GO-induced TLR4 signaling also activated MyD88 and TRIF, which recruited TRAF6 and Beclin 1 to initiate autophagy (Fig. 8).

Intriguingly, GO also elicited autophagy via the TLR9 pathway (Fig. 7D–G). This finding was contradictory to the previous report that TLR9 ligand (CpG oligonucleotide) failed to elicit autophagy [16,17], probably due to the difference in the type and concentration of agonist. Since both TLR4 and TLR9 pathways are similar in the MyD88-dependent arm with regard to signal transduction through MyD88 and TRAF6 activation, one can envisage that GO engagement of TLR9 activated MyD88 and TRAF6, leading to Beclin 1 and LC3 activation and subsequent autophagy (Fig. 8). Nonetheless, it should be noted that autophagy can be induced via stress signals such as phagocytosis [13], AIM2 inflammasome formation [24] and activation of Akt-TOC1/2-mTOR pathway [10]. It was also recently shown that nanomaterials (e.g. starburst polyamidoamine dendrimer and carbon nanotube) induce autophagy via the Akt-TSC1/2-mTOR signaling pathway [29,32] and gold nanoparticle-induced autophagy was associated with oxidative stress [31]. Therefore, the possibility that GO-induced autophagy via mechanisms other than TLR4 and TLR9 signaling cannot be excluded.

5. Conclusions

In summary, this study demonstrated that treatment of cells with GO simultaneously triggers autophagy and TLR4/TLR9-regulated inflammatory responses, and the autophagy was at least partly regulated by the TLRs pathway. Since TLRs-regulated autophagy can contribute to efficient autophagic elimination of intracellular microbes such as *Bacillus Calmette-Guerin* and *Listeria monocytogenes*, it is likely that GO-triggered autophagy is exploited by the cells to clear the internalized GO. However, this hypothesis awaits further experimental confirmation. Very importantly, TLRs are well known detectors for various biological molecules, but their sensing of non-living nanomaterials such as GO has yet to be reported. Neither has any study documented that nanomaterials can induce autophagy via the regulation of TLRs. This study thus suggests a mechanism by which cells respond to nanomaterials and underscores the importance of future safety evaluation of nanomaterials.

Acknowledgment

The authors acknowledge the financial support from the National Tsing Hua University (Booster Program 99N2544E1 and Toward World-Class University Project 100N2050E1, 101N2060E1) and National Science Council (99-2221-E-007-025-MY3, 100-2628-E-007-029-MY2, 100-2325-B-080-001), Taiwan.

Appendix A. Supplementary data

Supplementary data related to this article can be found online at doi:10.1016/j.biomaterials.2012.05.064.

References

[1] Liu Q, Shi J, Sun J, Wang T, Zeng L, Jiang G. Graphene and graphene oxide sheets supported on silica as versatile and high-performance adsorbents for solid-phase extraction. Angew Chem Int Ed Engl 2011;50:D5913–7.
[2] Kim H, Namgung R, Singha K, Oh IK, Kim WJ. Graphene oxide-polyethylenimine nanoconstruct as a gene delivery vector and bioimaging tool. Bioconjug Chem 2011;22:2558–67.
[3] Wang Y, Li Z, Hu D, Lin CT, Li J, Lin Y. Aptamer/graphene oxide nanocomplex for in situ molecular probing in living cells. J Am Chem Soc 2010;132:9274–6.
[4] Chen GY, Pang DWP, Hwang SM, Tuan HY, Hu YC. A graphene-based platform for induced pluripotent stem cells culture and differentiation. Biomaterials 2012;33:418–27.
[5] Zhang L, Lu Z, Zhao Q, Huang J, Shen H, Zhang Z. Enhanced chemotherapy efficacy by sequential delivery of siRNA and anticancer drugs using PEI-grafted graphene oxide. Small 2011;7:460–4.
[6] Zhang L, Xia J, Zhao Q, Liu L, Zhang Z. Functional graphene oxide as a nanocarrier for controlled loading and targeted delivery of mixed anticancer drugs. Small 2010;6:537–44.
[7] Yang K, Wan J, Zhang S, Tian B, Zhang Y, Liu Z. The influence of surface chemistry and size of nanoscale graphene oxide on photothermal therapy of cancer using ultra-low laser power. Biomaterials 2012;33:2206–14.
[8] Munz C. Enhancing immunity through autophagy. Annu Rev Immunol 2009;27:423–49.
[9] Dalby KN, Tekedereli I, Lopez-Berestein G, Ozpolat B. Targeting the prodeath and prosurvival functions of autophagy as novel therapeutic strategies in cancer. Autophagy 2010;6:322–9.
[10] Levine B, Mizushima N, Virgin HW. Autophagy in immunity and inflammation. Nature 2011;469:323–35.
[11] Ishii KJ, Koyama S, Nakagawa A, Coban C, Akira S. Host innate immune receptors and beyond: making sense of microbial infections. Cell Host Microbe 2008;3:352–63.
[12] Takeuchi O, Akira S. Pattern recognition receptors and inflammation. Cell 2010;140:805–20.
[13] Sanjuan MA, Dillon CP, Tait SW, Moshiach S, Dorsey F, Connell S, et al. Toll-like receptor signalling in macrophages links the autophagy pathway to phagocytosis. Nature 2007;450:1253–7.
[14] Xu Y, Jagannath C, Liu XD, Sharafkhaneh A, Kolodziejska KE, Eissa NT. Toll-like receptor 4 is a sensor for autophagy associated with innate immunity. Immunity 2007;27:135–44.
[15] Anand PK, Tait SW, Lamkanfi M, Amer AO, Nunez G, Pages G, et al. TLR2 and RIP2 pathways mediate autophagy of *Listeria monocytogenes* via extracellular signal-regulated kinase (ERK) activation. J Biol Chem 2011;286:42981–91.
[16] Delgado MA, Elmaoued RA, Davis AS, Kyei G, Deretic V. Toll-like receptors control autophagy. EMBO J 2008;27:1110–21.
[17] Shi CS, Kehrl JH. MyD88 and TRIF target Beclin 1 to trigger autophagy in macrophages. J Biol Chem 2008;283:33175–82.
[18] Shi CS, Kehrl JH. TRAF6 and A20 regulate lysine 63-linked ubiquitination of Beclin-1 to control TLR4-induced autophagy. Sci Signal 2010;3:ra42.
[19] Xu CF, Liu J, Hsu LC, Luo YP, Xiang R, Chuang TH. Functional interaction of heat shock protein 90 and Beclin 1 modulates toll-like receptor-mediated autophagy. FASEB J 2011;25:2700–10.
[20] Hummers WS, Offeman RE. Preparation of graphitic oxide. J Am Chem Soc 1958;80:1339.
[21] Fan XB, Peng WC, Li Y, Li XY, Wang SL, Zhang GL, et al. Deoxygenation of exfoliated graphite oxide under alkaline conditions: a green route to graphene preparation. Adv Mater 2008;20:4490–3.
[22] Zhou XS, Wu TB, Hu BJ, Yang GY, Han BX. Synthesis of graphene/polyaniline composite nanosheets mediated by polymerized ionic liquid. Chem Commun 2010;46:3663–5.
[23] Into T, Inomata M, Takayama E, Takigawa T. Autophagy in regulation of toll-like receptor signaling. Cell Signal 2012;24:1150–62.
[24] Shi CS, Shenderov K, Huang NN, Kabat J, Abu-Asab M, Fitzgerald KA, et al. Activation of autophagy by inflammatory signals limits IL-1β production by targeting ubiquitinated inflammasomes for destruction. Nat Immunol 2012;13:255–63.
[25] Li H, Li Y, Jiao J, Hu HM. Alpha-alumina nanoparticles induce efficient autophagy-dependent cross-presentation and potent antitumour response. Nat Nanotechnol 2011;6:645–50.
[26] Seleverstov O, Zabirnyk O, Zscharnack M, Bulavina L, Nowicki M, Heinrich JM, et al. Quantum dots for human mesenchymal stem cells labeling. A size-dependent autophagy activation. Nano Lett 2006;6:2826–32.
[27] Uematsu S, Akira S. Toll-like receptors and type I interferons. J Biol Chem 2007;282:15319–23.
[28] Kumagai Y, Takeuchi O, Akira S. TLR9 as a key receptor for the recognition of DNA. Adv Drug Deliv Rev 2008;60:795–804.
[29] Li C, Liu H, Sun Y, Wang H, Guo F, Rao S, et al. PAMAM nanoparticles promote acute lung injury by inducing autophagic cell death through the Akt-TSC2-mTOR signaling pathway. J Mol Cell Biol 2009;1:37–45.
[30] Zhang Q, Yang W, Man N, Zheng F, Shen Y, Sun K, et al. Autophagy-mediated chemosensitization in cancer cells by fullerene C60 nanocrystal. Autophagy 2009;5:1107–17.
[31] Li JJ, Hartono D, Ong CN, Bay BH, Yung LY. Autophagy and oxidative stress associated with gold nanoparticles. Biomaterials 2010;31:5996–6003.
[32] Liu H-L, Zhang Y-L, Yang N, Zhang Y-X, Liu X-Q, Li C-G, et al. A functionalized single-walled carbon nanotube-induced autophagic cell death in human lung cells through Akt–TSC2-mTOR signaling. Cell Death Dis 2011;2:e159.
[33] Yue H, Wei W, Yue Z, Wang B, Luo N, Gao Y, et al. The role of the lateral dimension of graphene oxide in the regulation of cellular responses. Biomaterials 2012;33:4013–21.
[34] Akira S, Uematsu S, Takeuchi O. Pathogen recognition and innate immunity. Cell 2006;124:783–801.
[35] Shi CS, Kehrl JH. Traf6 and A20 differentially regulate TLR4-induced autophagy by affecting the ubiquitination of Beclin 1. Autophagy 2010;6:986–7.